Preneural limitations on letter identification in central and peripheral vision

Paul J. Beckmann and Gordon E. Legge

Department of Psychology, University of Minnesota, 75 East River Road, Minneapolis, Minnesota, 55455

Received October 31, 2001; revised manuscript received July 1, 2002; accepted July 5, 2002

We created a sequential ideal-observer model that could address the question, How much of letter identification performance and its change with eccentricity can be accounted for by preneural factors? The ideal-observer model takes into account preneural factors including the stimulus rendering properties of a CRT display, the optical imaging quality of the eye, and photon capture and sampling characteristics of the cones. We validated the formulation of the model by comparing its performance on simple psychophysical tasks with that of previous sequential ideal-observer models. The model was used to study properties of the image rendering of letters. For example, the model's identification of high-resolution letters (i.e., many pixels per letter), but not low-resolution letters, is largely immune to changes in pixel width. We compared human and ideal-observer letter-identification acuity for the lowercase alphabet at 0°, 5°, and 20° retinal eccentricity. Acuity of the ideal observer for high-contrast letters is approximately seven times better than that of the human observers at 0°. Acuity decreased with eccentricity more rapidly for human observers than for the ideal observer such that the thresholds differed by a factor of 50 at 20°. A decrease in stimulus duration from 100 to 33 ms resulted in no decrease in *relative* threshold size between the human and ideal observers at all eccentricities, indicating that humans effectively integrate stimulus information over this range. Decreasing contrast from 75% to 25%, however, reduced the difference in acuities twofold at all eccentricities between humans and the ideal-observer model, consistent with the presence a compressive nonlinearity only in the human observers. The gap between human and ideal acuity in central vision means that there are substantial limitations in human letter recognition beyond the stage of photoreceptor sampling. The increasing performance gap between human and ideal-observer performance with eccentricity implicates an increasing role of neural limitations with eccentricity in limiting human letter identification.

OCIS codes: 330.0330, 330.4060, 330.1070.

1. INTRODUCTION

Many aspects of the early visual system change with eccentricity, including preneural factors such as optical imaging quality,[1–5] photoreceptor density,[6] the sampling aperture of the individual cones,[7,8] and the proportion of long (L)-, medium (M)-, and short (S)-, wavelength-sensitive cones.[9,10] Early stages of neural processing, including ganglion cell pooling, are also affected by eccentricity.[11]

Our focus in this paper is on the role of preneural visual factors in letter identification in central and peripheral vision. Ultimately, we hope to relate our findings to known limitations on reading performance in peripheral vision.[12,13] Letter-identification acuity, that is, the reciprocal of letter size at threshold, decreases with eccentricity.[14–18] In this paper we investigate how much of the change in letter-identification performance with eccentricity can be accounted for by corresponding changes in preneural factors, specifically, changes in optical imaging quality of the eye, and capture and absorption of light in the photoreceptor mosaic of the retina.

Table 1 summarizes important aspects of selected studies of letter identification in peripheral vision.[14,15,19–23] The study reported in this paper differs from this body of work in the following important ways. First, it measures letter identification by using the entire lowercase alphabet over a range of eccentricities. Second, it controls for pupil diameter, an important factor affecting imaging quality, without use of an external, artificial pupil. Third, it removes the effects of chromatic aberration by using stimuli with narrow-wavelength spectra.

We developed an ideal-observer model to investigate letter identification in central and peripheral vision. Geisler[24] coined the term "sequential ideal observer" to describe a framework in which a visual task is represented as a series of transformations in the early visual system, followed by a decision stage. We used this framework because it explicitly represents the physiological and optical changes in the early visual system from central to peripheral vision. Using the performance of this model as a benchmark, we can address how much the change in human letter-identification performance is driven by changes in the imaging quality of the eye and the sampling characteristics of the cone mosaic. This model extends the previous work by Geisler and colleagues in central vision[24–27] and Banks *et al.* in central and peripheral vision[28] in three important ways. First, it extends their two-alternative forced choice (2-AFC) formulations to *N*-alternative forced choice (*N*-AFC), enabling it to measure letter-identification performance using the full alphabet. Second, it represents the imaging quality of the eye across the visual field without the use of external artificial pupils. Analysis with artificial pupils, though convenient from an optics point of view, is less relevant to our long-term interest in peripheral letter recognition in reading. Third, the current model extends the transformational approach inherent in the sequential ideal-observer framework into the stimulus generation

domain by making explicit the rendering of letters on a pixel-based CRT display. This property makes the model suitable for studying the effect on letter recognition of the rendering characteristics of such displays.

Our interests in letter recognition in peripheral vision and reading are linked in the following way. Peripheral vision participates in the reading process since not only the centrally fixated letter but also eccentric letters may be acquired in one fixation.[13,29] Peripheral vision is especially important in reading with visual impairment that is due to central-field loss, where all the reading is done in the periphery.[30–32]

The remainder of the paper follows this plan: First, the details of the model are presented. We then present comparisons of the performance of this new model with its predecessors and an example of its application to the effects of stimulus rendering on performance. Next we describe an experiment measuring human letter identification in central and peripheral vision. The measured human performance is compared with the performance of our model. The paper ends with a general discussion.

2. STRUCTURE OF THE MODEL

Figure 1 illustrates that the model decomposes the task of letter identification into stages of stimulus rendering, retinal image formation, and image sampling. The first stage, consisting of three transformations, builds a spatiotemporal representation of the stimulus rendered on a monochrome display monitor. The second stage transforms this external stimulus into a retinal image, and the third stage forms a pattern of photons absorbed by cones within a synthesized patch of photoreceptors.

Table 2 summarizes important characteristics of the Geisler, Banks, and current models. Geisler[26] formulated his model for central vision only. To represent the characteristics of the eye's imaging system, he used the line-spread function of Campbell and Gubisch[2] for 2-mm pupils to form the point-spread function (PSF). The model of the retinal sampling was simplified.[33] He formulated the model for 2-AFC tasks[34] and measured the model's performance on a number of simple psychophysical tasks.

Banks and his colleagues[28] extended the sequential ideal-observer into the periphery (0°–40°). The model used more-restrictive optics,[35] resulting in a high-spatial-frequency cutoff at 48 cycles per degree[36] (cpd). However, the sampling of the retinal image was more sophisticated than Geisler's.[37] Banks measured the contrast-sensitivity function (CSF) of the model and of humans by using a half-cosine-enveloped circular sinewave-grating patch with a constant number of cycles.

Our model, like those of Geisler and Banks, uses the photon absorptions within each of the cone photoreceptors in a synthesized mosaic as the input to a decision stage.[38] The model's performance reveals how much task-relevant

Table 1. Aspects of Some of the Studies of Identification Performance in the Periphery or of Lowercase Letter Identification

Study	Number of Optotypes	Optotype Set	Eccentricities Measured (deg)	Time (ms)	Pupil Diameter	Foreground cd/m^2	Background cd/m^2
Beckmann and Legge (this paper)	26	Lowercase times	0, 5, 20	100	4 mm	300	30
Ludvigh[15]	5	Snellen (F, E, C, L, T)	0–10	[a]	[a]	black ink	30
Bouma[19]	25	Lowercase Courier	0–11	200	[a]	black ink	60
Anstis[14]	26	Uppercase Helvetica	0–60	[a]	[a]	black ink	21.6
Sanford[21]	26	Lowercase Snellen	0	[a]	[a]	black ink	white paper
Roethlein[20]	1352	26 type faces, both uppercase and lowercase	0	[a]	[a]	black ink	white paper
Seiple *et al.*[74]	9	Sloan	0–22	variable	[a]	73	46
van Nes[72]	25	Lowercase Courier	0–3	100	[a]	black ink	variable

[a] Uncontrolled.

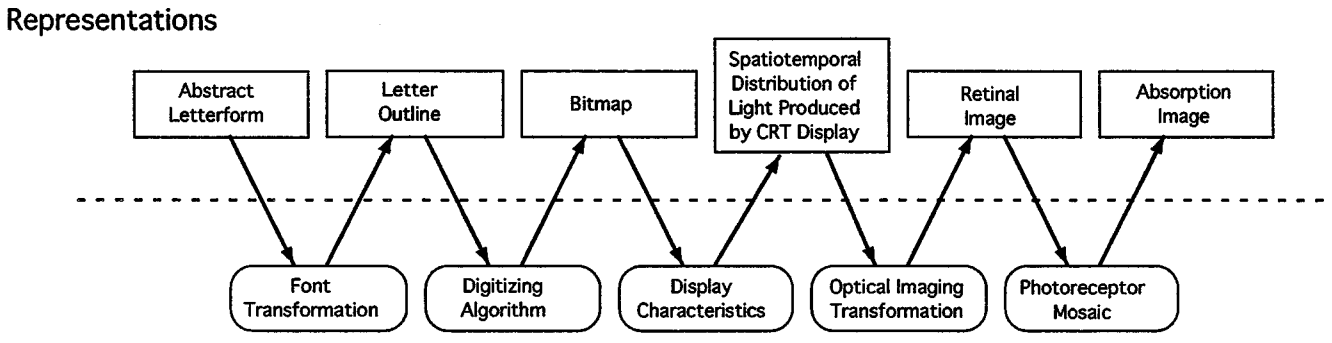

Fig. 1. Representations of the stimulus and the stages of the model that convert one representation to another.

Table 2. Key Characteristics of the Current Model and Closely Related Earlier Models in the Literature

Characteristic	Geisler[24]	Banks *et al.*[28]	This Paper
Eccentricity	Foveal	0°, 2°, 5°, 10°, 20°, 40°	0°, 5°, 20°
Stimulus			
Type	Fourier	Fourier	Bitmap
Rendering	None	None	CRT (Gaussian pixel)
Wavelength	Monochromatic	White	Monochromatic, extendable[b]
Optics			
PSF	Sum of two Gaussians	Diffraction-limited 1.5 mm	Sum of two Gaussians
based on	Campbell and Gubisch[2]	Wave theory	Navarro *et al.*[4]
Photoreceptor mosaic			
Geometry	Triangular close-packed	Triangular	Eccentricity dependent
Anatomical diameter	Fixed	ISD and OSD[a]	ISD[a]
Aperture	Cylindrical	Cylindrical	Gaussian
Position jitter	None	None	Eccentricity dependent
Isomerization rate	Fixed	Eccentricity dependent	Fixed
Decision rule			
Type	2-AFC[a]	2-IFC[a]	N-AFC[a]
Noise	Poisson @ receptor	Poisson @ receptor	Poisson @ receptor

[a] ISD, inner segment diameter; OSD, outer segment diameter; AFC, alternative forced-choice paradigm; IFC, interval forced-choice paradigm.
[b] Although the model is monochromatic, it has been structured in a way that its extension to polychromatic stimuli is relatively straightforward.

information is contained at the input to the decision stage, that is, at the level of photon absorption in the retinal cones.

This sequential ideal-observer approach stands in contrast to ideal-observer models that factor out effects of the early visual system, typically by adding external noise to the stimulus.[39] The addition of luminance noise swamps the noise in early vision and probes statistical efficiency at a decision stage that occurs later in the visual system. Letter-identification performance of this type of model is generally measured as a function of signal-to-noise ratio[40] (SNR). Our approach in the present paper focuses on the characteristics of the early, preneural visual system with the only noise limitation arising from the photon flux.

A. Formulation of the Model

1. Stimuli

Letter stimuli are frequently generated on a CRT-based display system. This generation process, represented by the first three transformations in Fig. 1, converts an abstract outline for a letter in a particular font into the spatiotemporal pattern of light actually presented to the participant. The pattern of stimulus light presented for any given letter depends on the shape of that letter within the typeface used (e.g., Courier), the characteristics of the signals generated by the computer's display electronics, and how the display device converts those signals into light.[41] The model represents the light produced by each pixel as a two-dimensional (2D) Gaussian spatial intensity distribution.[42] The bitmaps are displayed on the CRT for a fixed duration and are superimposed on an unstructured field of veiling light bright enough to stimulate photopic vision.

2. Optical Image Formation

The spatiotemporal pattern of light of a stimulus is imaged on the retinal surface by the optics of the eye. Figure 2 illustrates a number of PSF profiles relevant to our model. We used the data reported by Navarro *et al.*,[4] who used the method of Santamaría *et al.*[43] to assess the optical quality of the eye with natural pupil and accommodation.[44] The field scale of the eye was calculated for each eccentricity,[48] (see Table 3). The eye contains longitudinal and transverse chromatic aberration.[51–53] The current model avoids these effects by restricting its scope to monochromatic stimuli. We performed the human experiments under corresponding conditions (see Section 3).

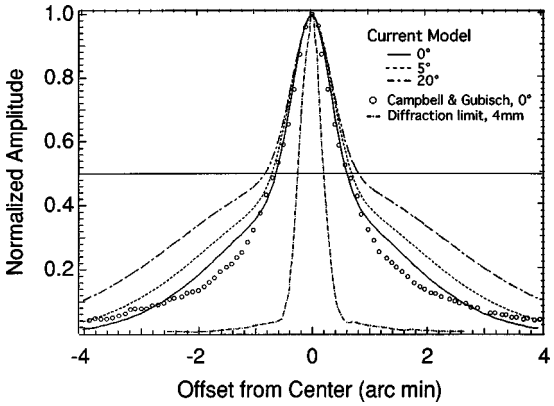

Fig. 2. PSFs used in the model are shown for 0°, 5°, and 20° eccentricity. They were derived from Navarro *et al.*[4] by using a sum of two Gaussian functions. In addition, the data of Campbell and Gubisch[2] for a 3.4-mm pupil in white light and the diffraction limit for a 4-mm pupil are shown. The curves shown have been normalized to a peak amplitude of 1.0 to emphasize the differences in their shapes.

3. Image Sampling by the Retina

We consider photopic vision and sampling by the cones only. The size of the light-collecting aperture of the cones and the spacing between individual cones increases with eccentricity. Psychophysical studies[8] have demonstrated that the size of this aperture is directly proportional to

the cross section of the cone's inner segment. The cross section of the cones changes from central to peripheral retina. The capture area of the sampling units in our model used the inner-segment diameters that Curcio measured across the human retina.[54]

Using histological methods, Curcio found a threefold variation in the peak density of cone photoreceptors (100,000–300,000/mm^2) from individual to individual.[6] The findings of Marcos and her colleagues using living eyes[55] supported those of Curcio. The simulations presented here use an intermediate peak value of 200,000/mm^2. The geometry of the mean cone position varies with eccentricity, in a tight-packed triangular mosaic in the central fovea and in a diamond mosaic in the far periphery.[50] The positions of individual cones depart from this arrangement, perturbed by a spatial jitter with a Gaussian distribution of zero mean and an eccentricity-dependent standard deviation. We arranged the sampling units within our model in this way.

The distribution of the three cone classes changes with eccentricity as well. The S-cone submosaic density has been measured directly.[9] Other psychophysical studies have placed the ratio of L:M cones very close to 2:1[56–58] and have shown this ratio to be constant across the retina.[59] Roorda and Williams,[60] using direct imaging techniques, have recently shown that considerable variability in this ratio exists in subjects with normal color vision. The L:M cone ratio for the two subjects of their study were 1.2:1 and 3.6:1. The work reported here will be based on an intermediate 2:1 L:M cone ratio.

Figure 3 shows examples of cone photoreceptor mosaics synthesized by the current model. The receptor locations are determined by using the algorithm outlined by Curcio and Sloan.[50] The geometry, the inner-segment diameter, and the jitter vary with retinal eccentricity. The assignment of any particular cone to the S, M, or L class is determined by a random draw, weighted by the proportion of the three classes at that cone's eccentricity.[61]

4. Cone-Class-Dependent Absorption Calculations

Following Geisler,[24] the absorption probability[62] for each cone class (S, M, L) is determined from the absorption data of Estevez.[64] The absorption of the macular pigment is insignificant at 555 nm, the wavelength considered here (see Wyszecki and Stiles,[64] p. 721). The unbleached fraction of cone photopigment for the anticipated 10–100-cd/m^2 background luminance range varies from 99.4 to 94.1%. The effects of cone bleaching are ignored in the simulations reported here.

5. Computational Approach

For each CRT pixel, the model first performs the spatial convolution of the pixel luminance function and the eye's PSF. The result is the pixel's light distribution on the retinal surface. Then the distance between the center of a pixel image and the center of each photoreceptor aperture is calculated. This distance is used to calculate the convolution of the aperture of the photoreceptor and the pixel image on the retina. For each photoreceptor, the integral of this convolution is proportional to the mean number of photons captured by the photoreceptor from the pixel. The model exploits the Gaussian representations of the pixel profile, the optical PSF of the eye, and the photoreceptor aperture to make closed-form calculations strictly in the spatial domain.

In this way, the model calculates a transfer vector (see Appendix A) from each pixel on the CRT to the entire photoreceptor mosaic of the retinal patch. The elements of this vector represent how much of the light from that pixel is received by each photoreceptor in the mosaic. An entire stimulus pattern is represented by a bitmap, i.e., a set of scaling factors for the peak luminance of each pixel. To calculate the photons captured for each photoreceptor from a displayed stimulus, then, the transfer vector for each pixel is multiplied by that pixel's peak luminance in the bitmap being considered. The photons contributed by that pixel in the bitmap are added to the photons con-

Table 3. Optical and Retinal Parameters at 0°, 5°, and 20° Eccentricity Used in the Simulations

Parameter	Eccentricity (deg) 0	5	20	Units
PSF[a]				
$\alpha 1$	0.570	0.546	0.497	
$\sigma 1$	0.348	0.369	0.356	Arc minutes
$\sigma 2$	1.530	1.804	2.262	Arc minutes
Photoreceptor patch				
Cone Density	200,000	18,000	3,000	Inverse square millimeters
Compression ratio[b]	0.760	0.838	0.900	
Jitter[b]	0.117	0.149	0.155	
Inner-segment diameter	2.23	6.98	8.10	Micrometers
Chen aperture σ	0.455	1.42	1.65	Micrometers
Cone proportions				
L-cone proportion	0.667	0.622	0.620	
M-cone proportion	0.333	0.311	0.310	
S-cone proportion	0.000	0.067	0.070	

[a] The parameters shown were determined by fitting the data in Fig. 2 with the sum of two Gaussians with a two-dimensional integral of 1.0.
[b] The parameters "compression ratio" and "jitter" are used in our receptor-mosaic synthesis routine after Curcio and Sloan.[50]

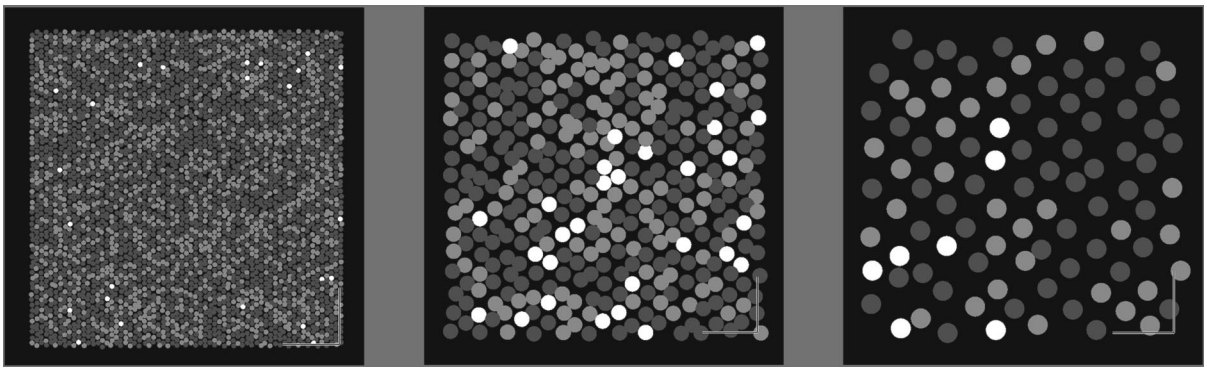

Fig. 3. Three synthetic cone mosaics at 0°, 5°, and 20° (left to right) with jitter. These mosaics were generated from the parameters in Table 3. S cones are the lightest gray and L cones the darkest, with M cones rendered at an intermediate level of gray. 25-μm bars are shown in the lower-right corner of each panel for reference.

tributed by other pixels. This procedure is performed over all pixels, with the contributions from each pixel accumulated in the captured photon count for each photoreceptor.

The photon count calculated in this way represents the mean number of photons captured by each photoreceptor for a stimulus presentation. The proportion of captured photons absorbed by the photoreceptor depends on the cone class and the wavelength of the photon. Quantum noise with Poisson statistics[65] is the only uncertainty that limits the performance of this ideal observer.

For a simulated trial, the model produces an absorption image in which each element represents the number of photons absorbed by a photoreceptor during the trial. (This image includes the contributions of quantum noise.) Given this absorption image, the model must decide which of N possible stimuli was most likely presented. To do this, the model uses precomputed image templates, one for each of the N possible stimuli. The elements of these templates represent the average number of photons absorbed by that receptor when that stimulus is present. The templates are used together with the trial absorptions in the mosaic photoreceptors to evaluate the likelihood of the absorptions arising from each possible stimulus letter. The model uses a weighted minimum-distance classifier[67] to make this decision. (See Appendix B for details.) The model is implemented in C on an SGI work station.

B. Validation of the Model

Our model follows directly from those of Geisler[24] and Banks,[28] and it is important to compare its performance with that of its predecessors. While the formulations are different, the underlying assumptions (e.g., Poisson quantum noise, sampling by photoreceptors, decision stage at the level of quantum absorption) are very similar. To validate the model, we compared its performance on intensity discrimination, two-dot discrimination, and contrast-sensitivity tasks.

1. Intensity Discrimination

Human performance in the intensity-discrimination task at low luminance levels follows the DeVries–Rose law $\Delta N/\sqrt{N} = k$, where N is the number of photons in the stimulus and ΔN is the threshold increment. This law is what would be expected from a system limited only by quantum noise. This would be the expected performance of the model since it is quantum noise limited at all luminance levels. We verified this with its performance, over a 4-log-unit range of total absorbed photons, which fell close to the DeVries–Rose law behavior of Geisler's model for which $\Delta N/\sqrt{N} = 1.36$.

Since this task depends only on intensity differences and not on spatial factors, these results validate the N-AFC formulation of the decision stage as equivalent to the 2-AFC decision stage of Geisler's model.

2. Two-Point Resolution

The two-point resolution task furthers the verification by examining the interplay between the model's optical imaging and retinal sampling. The model's task was to discriminate between two stimuli. One stimulus was a single pixel in the center of the display. The other stimulus consisted of two pixels, equally spaced left and right of the position of the center pixel, both with 1/2 the intensity of the pixel in the first stimulus. The stimuli were presented at 0°, 5°, and 20° eccentricity, with no veiling light, for 0.1 s. Each pixel subtended 41 arc sec (± 2 standard deviations of diameter). The threshold separation of the two pixels in the second stimulus (75% correct performance) was determined at a number of levels of absorbed photons.

For a mean of 50 absorbed quanta for the single-dot stimulus (25 each for the two-dot stimulus) the threshold separation was 60 arc sec for all three eccentricities. Threshold separation dropped to 20 arc sec for a mean of 5000 absorbed quanta from the stimuli.

The performance of the current model at all three eccentricities closely matches the performance of Geisler's model in central vision with a 0.25-arc-min optical blur. The threshold separation varies with the $-1/4$ power of intensity, similar to Geisler's model in central vision.

Our model's performance in central vision and that of Geisler's model match across a wide range of quantal absorptions. However, the constancy of threshold separations with eccentricity in our model is puzzling for two reasons. First, the proportion of the retinal surface not occupied by cone apertures increases considerably from central vision to 20° eccentricity, presumably making it harder to detect dots. The two-dot resolution perfor-

mance, however, is evaluated in terms of *absorbed* quanta, not stimulus quanta. In addition, because the point-source images are circular and cover a great many cones, even in peripheral vision, the model is likely making use of small differences in the absorbed photon patterns of one- and two-dot patterns to support its decision. Second, imaging quality is often thought to decline with eccentricity, with an adverse effect on two-dot resolution. Navarro *et al.*[4] found, however, that optical imaging quality declined slowly with eccentricity.

It is a surprising result of our analysis that ideal-observer performance is immune to retinal eccentricity out to 20°, at least when performance is measured in terms of absorbed photons.

3. Contrast-Sensitivity Function

Banks and colleagues measured the contrast sensitivity of his version of the ideal-observer model in central and peripheral vision.[28,68] To compare the pattern-vision performance of his model with that of ours, we measured the CSF of our model at 0°, 5°, and 20° eccentricity using the same stimuli that Banks used.

The model performed a two-AFC detection task under conditions similar to those used by Banks. One stimulus was a 7.5-cycle Gabor patch.[69] The other stimulus field was the same size and blank. The presentation was 0.1 s long on an unstructured background of 340 cd/m^2. The threshold criterion was 75% correct.

The results of the simulations are shown in Fig. 4. At 0°, the contrast sensitivity declines from 1000 at 10 cpd to 100 at 30 cpd. The values at 5° follows this same pattern. For 20° eccentricity, the CSF declines from 400 at 10 cpd to 40 at 30 cpd. The cutoff spatial frequencies were 78, 61, and 55 cpd at 0°, 5°, and 20°.

The sensitivities of the current model are similar to those found by Banks. Notably, however, the CSF cutoffs for the current model are higher. Banks's CSF cutoff depends more strongly on eccentricity, 60 cpd at 0° dropping to ~20 cpd at 20°. Consideration of diffraction limits[70] would place the cutoff between 62.5 and 110 cpd. The cutoff frequency of our model at all eccentricities is within this range.

4. Summary

We tested our model with tasks performed by previous sequential ideal-observer models. Square-root-law performance for intensity discrimination was identical to that of Geisler's model, with the same constant of proportionality. Two-dot resolution performance was identical to that of Geisler over a 4-log-unit range of absorbed quanta. Contrast sensitivity across eccentricity was comparable to that found by Banks[28] but with systematically higher cutoff frequencies for the current model than those of Banks.

C. Application to Rendering of Small Letters

One of the unique aspects of the current model is the attention paid to the rendering of the stimulus. The model can be used to show how changes in rendering of characters affect the information available to early vision. We illustrate with one example. We ask, How is the model's letter acuity affected by the interaction of the width of the pixels with the number of pixels used to render letters?

1. Method

Lowercase Times-Roman letters were used as stimuli. Absorption template sets were generated by changing the rendering resolution (i.e., number of pixels per x height) and the pixel luminance profile. The visual letter size was changed by varying the viewing-distance parameter of the model, with the physical size of the letter remaining the same. The simulated trials consisted of a 100-ms presentation with a background luminance of 0.034 cd/m^2 and a foreground luminance of 0.34 cd/m^2. The Michel-

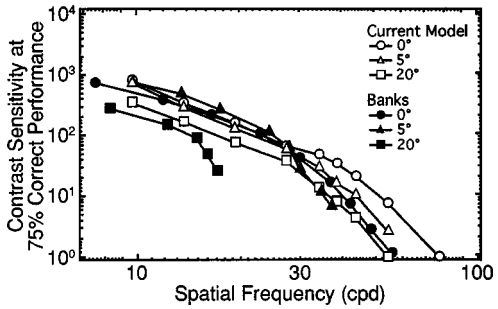

Fig. 4. Contrast-sensitivity performance of the model at 0°, 5°, and 20° eccentricity. The stimulus was a horizontal cosine grating modulated by a half-cosine envelope spanning 7.5 grating periods. The background luminance was 340 cd/m^2 and the exposure duration was 100 ms, with 400 simulated trials per point. The CRT pixel spacing was 1/7 mm and the spatial standard deviation of the pixel luminance profile was 0.1 mm. Data from Banks *et al.*[28] are shown for comparison.

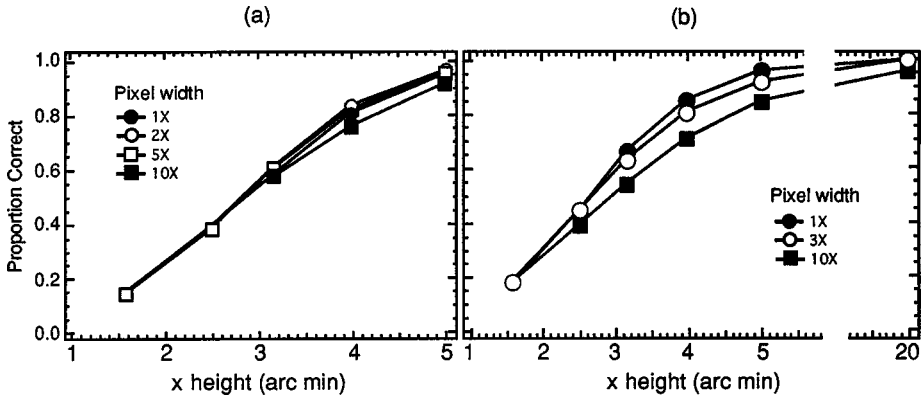

Fig. 5. Letter-identification performance as a function of visual size for letters of fixed physical size but different pixel profiles. (a) Letters rendered with 27 pixels over the height of a lowercase x. (b) Letters rendered with nine pixels over an x height, 100 simulated trials per point.

son contrast was 82%. For each condition, each letter of the alphabet was presented 100 times. The percent correct performance of the model was calculated.

2. Results

The effect of pixel width on the model's performance is summarized in Fig. 5(a). The letters with 27-pixel x heights were rendered with pixel-profile standard deviations of 1, 2, 5, and 10 times the pixel spacing. The physical height of the letter was constant, and the visual size of the letter was varied by changing the viewing distance.

Performance changed little with pixel width for 1.6- and 2.5-arc-min-high letters, with the spread widening slightly to ~2% at 3.1-arc-min letter size. Only a modest performance decrement occurred when the pixels were broadened to ten times the pixel spacing. The lack of effect is surprising given the amount of image degradation that these broad pixels induce. To investigate possible interaction between the rendering resolution and the effect of pixel profile, comparable simulations were run with the 9-pixel x-height letters. The results of these simulations are summarized in Fig. 5(b).

The expected degradation of performance by broad pixels is more apparent in Fig. 5(b). Even when the letters are four times the acuity limit, the ideal observer cannot reach 100% performance for the letters rendered with the broadest pixels. Thus broad pixels do affect the performance of the model for coarsely sampled letters but have little effect on performance for more finely sampled letters.

3. COMPARING HUMAN AND IDEAL LETTER RECOGNITION IN CENTRAL AND PERIPHERAL VISION

A. Introduction

How much of the change in human letter acuity from central to peripheral vision can be accounted for by changes in the optical imaging and photoreceptor sampling of the eye? To address this question, we measured human letter-identification performance at 0°, 5°, and 20° eccentricity. We compared human performance with the performance of our sequential ideal-observer model. To enhance the informativeness of the comparison, three aspects of the model and experiment were carefully matched in this study, namely, the stimulus generation,[42] the optical imaging of the eye,[4] and the sampling characteristics of the cone photoreceptors.[6,8–10,54,60]

Previous research[71–74] indicates that human letter recognition is largely independent of contrast above some critical level and largely independent of exposure time beyond some critical duration. On the other hand, we would expect an ideal observer to benefit from both increasing contrast and prolonged exposure time. To the extent that these expectations are confirmed, the difference between human and ideal letter recognition will depend on these two stimulus parameters. For this reason, we evaluated the effects of letter contrast (75% and 25%) and exposure time (100 ms and 33 ms) on human and ideal performance under conditions permitting a direct comparison. We are also interested in the effect of exposure time because of its relevance to reading speed.

B. Method

1. Stimuli

The stimulus set consisted of the 26 lowercase letters from the Postscript™ Times-Roman font. Three sets of letters with x heights of 20, 60, and 300 pixels were generated for use at 0°, 5°, and 20°.[75] (These sizes were chosen to approximate the differences in letter acuity at the three eccentricities.)

Bright letter images were generated by using an Electrohome CRT with a pixel pitch of 1/7 mm and an estimated pixel width of 0.1 mm. A 40-cd/m^2 stimulus background was generated with a slide projector and optically combined with letter images for presentation to the participant. The angular character size was controlled by varying the viewing distance while keeping the physical size of the letters constant. Before target presentation, a pattern of four inward-pointed arrowheads was displayed to cue the location of the upcoming letter for the participant. For presentations in the peripheral visual field, the participant used a white bowtie-shaped pattern as a fixation mark.[76,77] For foveal presentations, the pattern of arrowheads served as a fixation and accommodation target.

In the first experiment, psychometric functions (percent correct versus character size) were measured for high-contrast letters (75% Michelson contrast) presented for 100 ms. In the second and third experiments, psychometric functions were measured for reduced-contrast letters (25% Michelson contrast) presented for 100 ms and high-contrast letters presented for 33 ms.

2. Instrumentation and Procedure

A bite bar stabilized the participant's head for pupilometry. A view of the left eye was imaged as a reflection in a prism beam splitter positioned close to the eye. An ISCAN eyetracking system monitored the pupil diameter with infrared light. The luminance of a white surround was adjusted to keep the pupil at 4 mm (typically between 20 and 40 cd/m^2). When the pupil diameter was between 3.5 and 4.5 mm, a beep sounded and the stimulus was presented to the central (0°) or nasal (5°, 20°) visual field of the participant's left eye. The participant made letter-identification responses on a keyboard. Computer-generated voice verification was used to check for typing accuracy.

The 26 lowercase letters were presented in random order five times per block. Each session consisted of nine blocks. The block sequence rotated three times through

Table 4. Participant Summary

Subject	Age	Visual Acuity	Log Contrast Sensitivity
BJS	29	20/16	1.65
BLG	22	20/16	1.95
PJB[a]	45	20/16	1.80
TRS	23	20/12.5	1.80

[a] Wore corrective lenses during the experiment.

the three eccentricities of 0°, 5°, and 20° in that order but with a different starting eccentricity for each session. These nine blocks generated data for one character size at each eccentricity and lasted approximately 2 h. Between experimental sessions, the angular letter size for all three eccentricities was varied by changing the viewing distance.

3. Data Analysis

We fitted our psychometric functions with the Weibull function:

$$\pi(\sigma) = 1 - \{(25/26)*\exp[-(\sigma/\alpha)^{\beta}]\} \quad (1)$$

where σ = letter size, π = proportion correct, and β = slope parameter and when the guessing rate is 1/26 and the finger error rate is 0; $\pi(\alpha)=0.646$. We used resampling statistical methods[78,79] to evaluate the variability of the slope and threshold letter size estimates, using the Levenberg–Marquardt algorithm[80] to search for minimum chi-square.

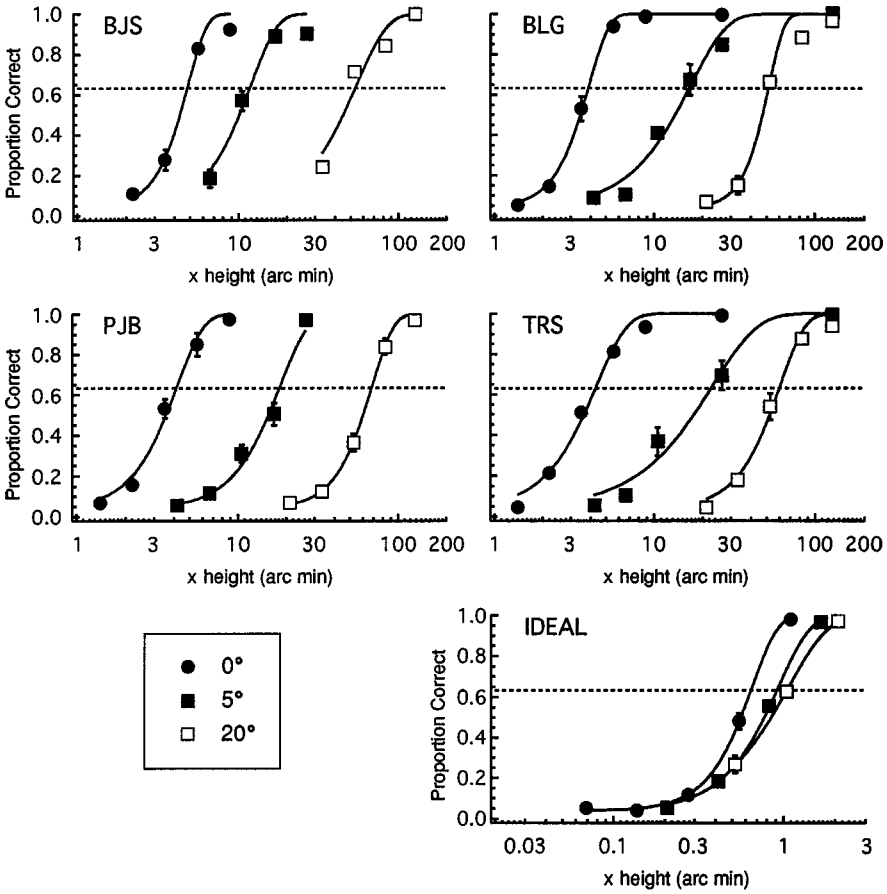

Fig. 6. Proportion correct as a function of letter x height in arc minutes for four human participants and the ideal-observer model (IDEAL). Psychometric data are given for 100-ms presentations at Michelson contrast of 75%. Mean performance is plotted for the three data blocks at 0°, 5°, and 20° eccentricity. Weibull-function fits to the block means are shown. Standard deviation bars are shown when they are larger than the symbols.

Table 5. Mean Weibull Slope Parameter (beta) and Threshold Letter Size (alpha) for the Three Experiments

Eccentricity (deg)	High Contrast/100 ms					Low Contrast/100 ms			High Contrast/33 ms		
	BGS	BLG	PJB	TRS	Ideal	BJS	PJB	Ideal	BJS	PJB	Ideal
Weibull Threshold Size (arc min)											
0	4.8	3.9	4.2	4.4	0.66	7.3	7.3	1.9	4.3	5	0.83
5	11.9	16.9	18.4	23.3	0.93	14.7	24.3	2.4	15.8	23.9	1.2
20	54.4	52.1	69.3	61.1	1.1	49.4	99.1	3	51.6	94.6	1.4
Weibull Slope Parameter											
0	3.7	3.4	2.6	2.3	2.8	2.9	3.1	3.1	3.6	2.9	2.7
5	2.6	1.9	2.5	1.5	2.3	2.8	3.1	3.1	2	2.4	2.6
20	2.3	4.6	3.2	2.8	1.8	3.8	3.5	2.9	4.8	2.6	2

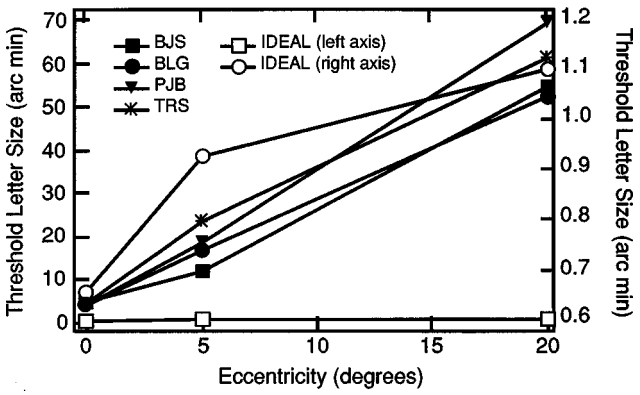

Fig. 7. Threshold letter size as a function of eccentricity for four human participants and the ideal-observer model. Standard deviations of the thresholds from resampling analysis are shown when they are larger than the symbol. The ideal-observer model data are shown at two different scales. The open squares show the data on the same scale as the human data (use the left-axis scale). The open circles show the data on an expanded scale to show detail (use the right-axis scale).

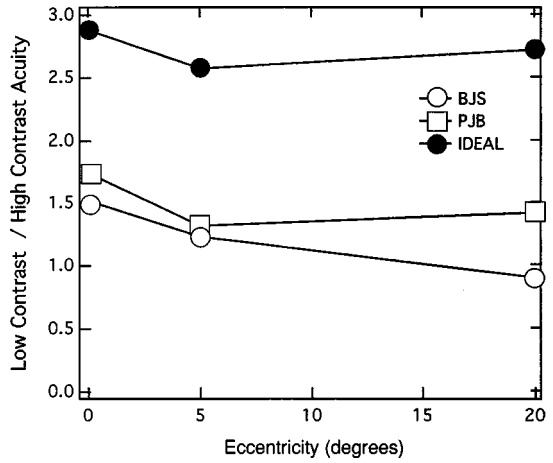

Fig. 8. Change in threshold letter size with a decrease in contrast from 75% to 25% with exposure time of 100 ms. The ratio of low-contrast threshold letter size over high-contrast threshold letter size as a function of eccentricity for two human participants and the ideal-observer model is shown.

4. Participants

Four observers with normal vision participated in the study. Table 4 summarizes their visual attributes. Acuities are stated for central vision of the left eye (the eye used in the experiment) as measured at 4 m with the Lighthouse ETDRS letter chart (2nd ed.). Contrast sensitivity was measured at 1 m with the Pelli–Robson Contrast Sensitivity chart. Participant PJB wore spectacles during the test and experiments. The other participants did not require refractive correction. Consent forms and experimental procedures were approved by the Human Subject Committee of the University of Minnesota. All participants gave informed consent.

C. Results

1. High-Contrast, 100-ms Presentation

Acuity psychometric functions for high-contrast letters, presented for 100 ms, are plotted in Fig. 6. Values for the Weibull threshold (α) and slope (β) are summarized in Table 5. The thresholds for the human participants follow a linear increase with eccentricity, with the best-fitting line having the form $\alpha = 3.78 + (2.76\,\eta)$ (Pearson's $r = 0.997$), where α is the threshold x height in arc minutes and η is eccentricity in degrees of visual angle. This reflects an E_2 value of 1.37°. The thresholds are plotted as a function of eccentricity in Fig. 7.

Note that the thresholds for the ideal-observer model are much smaller than those for the human observers. The ideal thresholds increase from 0° to 5° and then flatten from 5° to 20°.

The slopes of the psychometric functions for both humans and the model (Table 5) generally fell between 2.0 and 3.5, decreasing from 0° to 5°, and either remained constant or increased from 5° to 20°. This relatively small variability in slope means that our threshold comparisons across observers and eccentricities remain stable for different threshold criteria.

2. Lower Contrast and Shorter Presentation

Participants BJS and PJB performed letter identification under circumstances identical to those in the first experiment but with lower contrast. These measurements were made with contrast for the human observers at 19–27% and for the ideal observer at 20%. Performance data for these two participants and the ideal-observer model relative to that of the high-contrast condition are shown in Fig. 8. With reduction in contrast, threshold letter size increased 2.6 to 2.9 times for the ideal observer, depending on eccentricity, but only 25–74% for the two human participants in all but one case.

In addition, BJS and PJB performed letter identification under circumstances identical to those in the main experiment but with a shorter presentation time, 33 ms rather than 100 ms.[81] Performance data for these two participants and the ideal-observer model relative to that of the 100-ms condition are shown in Fig. 9. Threshold letter size for participant PJB increased 19–37% with de-

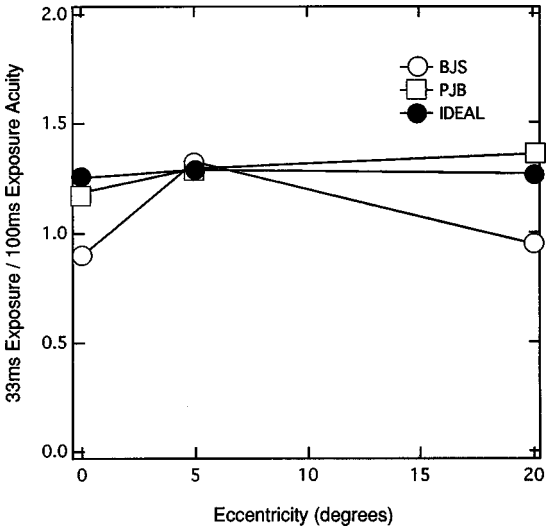

Fig. 9. Change in threshold letter size with a decrease in exposure time from 100 to 33 ms with contrast of 75%. The ratio of 33-ms threshold letter size over 100-ms threshold letter size as a function of eccentricity for two human participants and the ideal-observer model is shown.

creased exposure time. The effects of decreased exposure on the performance of participant BJS were mixed. With decreased exposure time from 100 to 33 ms, the threshold letter size of the model increased by 26–29%, depending on eccentricity. The effect of decreasing exposure time on PJB and the model were almost identical.

As in the main experiment, the weak effects of the stimulus parameters on slopes of the psychometric functions (Table 5) mean that comparisons of threshold values across conditions are fairly stable for different threshold criteria.

4. GENERAL DISCUSSION

The main goal of this paper was to compare the letter-identification performance of human observers in central and peripheral vision with that of an ideal-observer model of preneural vision. The human thresholds measured in this study are similar to those measured in other studies. For the Anstis[14] and Ludvigh[15] data, and for participants BJS and BLG in the current study, the threshold letter size grows from 4 arc min at 0° eccentricity to ~55 arc min at 20° (2.5 arc min/degree). For participants PJB and TRS, the threshold letter size grows from ~4 arc min at 0° to 60–70 arc min at 20° (3 arc min/degree). Despite the differences in character sets, viewing conditions, and threshold criteria, these studies yield generally similar results from 0° to 20°.

A. Differences in Central-Field Acuity of the Ideal and the Human Observers

The mean acuity letter size for the human observers at 0° for high-contrast letters is 6.6× larger than the threshold letter size for the ideal-observer model. What could explain this performance difference? We consider three possible factors: spatial uncertainty, contrast coding, and temporal integration.

One possible source of the acuity difference is spatial uncertainty in the human observers. In target-detection tasks, ideal-observer models improve on human performance by taking advantage of exact knowledge of the spatial locations of stimuli. For a human observer, the point of gaze drifts and exhibits high-frequency tremor during fixation.[82] The gaze drift would result in uncertainty in the nominal position of the stimulus image relative to the cone mosaic, and the tremor during fixation would result in additional blur. While spatial uncertainty in stimulus location is unlikely to be as important in an identification task, it is possible that this factor plays a role in accounting for a portion of the large difference between human and ideal acuities. Although we did not include spatial uncertainty in our simulations, we can estimate the magnitude of the effect from the work of Tjan.[83] Using an ideal-observer analysis and methods similar to those that he reported for object identification,[84] Tjan estimated the effect of positional uncertainty (related to the uncertainty generated by drift during fixation) on letter-identification performance.[85] Using Tjan's data, we estimate that positional uncertainty might increase the acuity-size letters for the ideal observer by ~33%. This is likely an underestimate of the effect of spatial uncertainty on the performance of our model, however, since Tjan's ideal-observer analysis was only of the external stimuli and was not limited either by the optics of the eye or the sampling of the retinal mosaic. Nevertheless, this analysis suggests that positional uncertainty plays only a minor role in accounting for the difference in human and ideal letter acuity in central vision.

The ideal-observer model contains no explicit contrast-processing stages. It implicitly represents contrast in the difference in captured photons across the mosaic. How does the reduction in stimulus contrast change the relationships between human and ideal threshold letter sizes? Reducing letter contrast from 75% to 25% decreased the ratio by a factor of approximately 2 at all eccentricities. This result shows that human acuity is closer to ideal values at low contrast, which implies that humans are inefficient in using the extra information associated with higher-contrast letters in improving acuity.

The effects of contrast reduction can be considered in the context of compressive contrast processing or contrast gain control. In this view, the weaker effect of contrast on human performance than on ideal performance is due to the operation of a nonlinear contrast-compression stage.[86] The model, however, has no such compressive nonlinearity, and its acuity has a stronger dependence on stimulus contrast.

How does the reduction in exposure time change the relationships between human and ideal threshold letter sizes? Figure 9 reveals that a change in exposure time from 100 to 33 ms resulted in an equivalent increase in the threshold letter size for both the model and participant PJB by ~30% at all three eccentricities. The effect on the acuity of BJS relative to the ideal was mixed.

The ideal-observer model contains no temporal-processing limitations. The signal strength associated with the stimulus accumulates as long as the stimulus is present with the SNR increasing as the square root of the accumulated photon count in the photoreceptors. The model has an infinite integration period; longer exposures improve SNR indefinitely. Participant PJB acted like an "integrator" for letter identification. The effect of exposure duration on the acuity of PJB paralleled its effect on the acuity of the ideal observer at all eccentricities.

To summarize, the sevenfold difference between human and ideal letter acuities in central vision is probably due at least in part to human spatial uncertainty and compressive-contrast coding in humans.

B. Differences in Peripheral-Field Acuity of the Ideal and Human Observers

Figure 10 shows the change in acuity for the four participants in the first experiment and the ideal observer, normalized to central acuity. For the human observers there is approximately a fourfold increase in threshold letter size at 5° with respect to 0° and a fourteen-fold increase at 20°. The ideal observer, however, exhibits only a 41% and 67% increase at 5° and 20°. Clearly, factors not represented in our model have important influences on peripheral human letter acuity. Presumably, these factors are neural in origin and postreceptoral. A candidate factor is the change in ganglion-cell density across the retina. When the threshold letter size of the ideal observer is multiplied by the ganglion-cell pooling factor es-

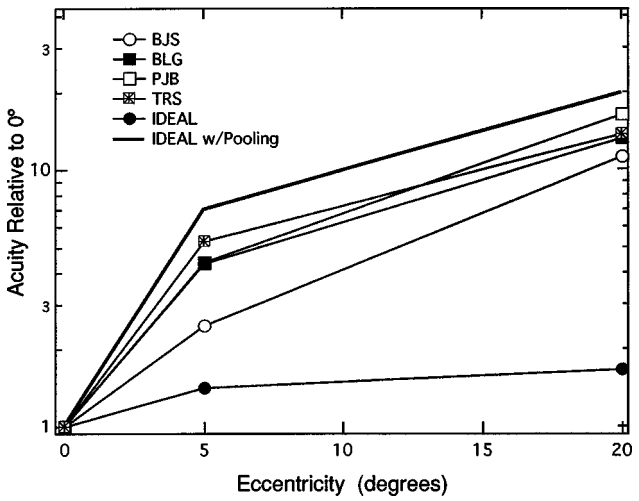

Fig. 10. Change in threshold letter size under high-contrast, 100-ms exposure conditions. Threshold letter size normalized to that at 0° for four human participants and the ideal-observer model is shown. In addition, the normalized threshold letter size for the model, multiplied by the estimate of ganglion-cell pooling of Banks *et al.*[28] is plotted.

timated by Banks,[28,87] threshold letter size increases approximately sevenfold at 5° and by approximately twentyfold at 20° with respect to 0°, quite close to the human values. Although no one has yet incorporated ganglion-cell processing into sequential ideal-observer models, ganglion-cell pooling may be an important determinant of changes in peripheral acuity.

In brief summary, we have developed a sequential ideal-observer model of letter acuity across the visual field. The model includes the preneural visual processes likely to affect letter recognition. The model's performance sets a standard that describes what would be expected if all the information present at the front end of neural processing were used optimally. Human acuity falls far short of this standard, with the difference increasing from central to peripheral vision. It is likely that a substantial portion of the neural-processing deficit occurs at early stages—effects of spatial uncertainty, contrast compression, and ganglion-cell pooling—although it remains possible that a portion of the deficit is attributable to higher-level decision stages.

APPENDIX A: FUNCTIONAL FORM OF THE TRANSFER MATRIX ELEMENTS

The Gaussian pixel radiance function $pixel(x, y)$ of amplitude *pamp* and spatial standard deviation *psd* is written

$$pixel(x, y) = pamp\left\{\left(\frac{1}{2\pi\ psd^2}\right)\exp\left(-\left[\frac{x^2 + y^2}{2\ psd^2}\right]\right)\right\}. \tag{A1}$$

The PSF is modeled as the sum of two Gaussians. Each component has horizontal and vertical spatial standard deviations *psfhsd* and *psfvsd* and is written

$$psf(x, y) = \left(\frac{1}{2\pi\ psfhsd\ psfvsd}\right) \times \exp\left(-\left[\frac{x^2}{2\ psfhsd^2} + \frac{y^2}{2\ psfvsd^2}\right]\right) \tag{A2}$$

The convolution produced the retinal intensity function:

$$retina(x, y) = pixel \otimes psf = \int\int_{-\infty}^{+\infty} pixel[(x - \eta), (y - v)]psf(\eta, v)\mathrm{d}\eta\mathrm{d}v. \tag{A3}$$

The receptor capture function with a standard deviation of *recepsd* and a peak of 1.0 (complete capture) can be written

$$capture(x, y) = \exp\left(-\left[\frac{x^2 + y^2}{2\ recepsd^2}\right]\right). \tag{A4}$$

Consider the centers of a pixel image and receptor aperture offset by x_0 and y_0. The amount of light captured by the receptor from the pixel is the integral of the product of the irradiance function and the aperture and can be shown to be

$$transfer(x_0, y_0) = \left(\frac{recepsd^2}{sh\ sv}\right)\exp\left(-\left[\frac{x_0^2}{2sh^2} + \frac{y_0^2}{2sv^2}\right]\right), \tag{A5}$$

where

$$sh = (psd^2 + psfhsd^2 + recepsd^2)^{1/2} \tag{A6}$$

and

$$sv = (psd^2 + psfvsd^2 + recepsd^2)^{1/2}. \tag{A7}$$

The ultimate transfer function is formed by superposition of the transfer functions arising from both of the Gaussian components of the PSF.

APPENDIX B: DECISION-STAGE CALCULATIONS

A template, made up of elements m_{ij} representing the mean number of photons absorbed in receptor j when stimulus i is presented, is precalculated for each possible stimulus. The model must evaluate the likelihood that a stimulus i has been presented given a pattern of photon absorptions Z_j, where j ranges over the receptors:

$$L_i = \prod_j p(m_{ij}|Z_j). \tag{B1}$$

Since log likelihood is monotonic with likelihood and we require only a ranking of the likelihood values, we calculate an equivalent likelihood measure:

$$l_i = \ln(L_i) = \sum_j \ln(p(m_{ij}|Z_j). \tag{B2}$$

For the Poisson equation,

$$\ln[\,p(m_{ij}|Z_j)\,] = \frac{m_{ij}^{Z_j}\exp(-m_{ij})}{Z_j!} \quad \text{(B3)}$$

For Z_j less than 11, Eq. (B3) is used to compute the contribution of receptor j to the likelihood. For Z_j of 11 and greater, the Gaussian approximation to the Poisson distribution can be used. For those receptors, the contribution to l_i is computed as

$$\begin{aligned} l_i &= \ln[\,p(m_{ij}|Z_j)\,] \\ &= \ln\left\{\left(\frac{1}{\sqrt{2\pi m_{ij}}}\right)\exp\left(-\left[\frac{(Z_j - m_{ij})^2}{2m_{ij}}\right]\right)\right\} \\ &= -0.5\ln(2\pi) - 0.5\ln m_{ij} - \left[\frac{(Z_j - m_{ij})^2}{2m_{ij}}\right]. \end{aligned} \quad \text{(B4)}$$

ACKNOWLEDGMENTS

This research was supported by National Institutes of Health grant EY-02934 to Gordon E. Legge. We thank Bill Geisler, Dan Kersten, and Marty Banks for helpful discussions. We thank Bosco Tjan for sharing his data and for many helpful discussions. We also thank Steve Mansfield for his help with resampling techniques. Finally, a special thanks goes to BJS for participating in all three experiments. Earlier versions of this work were presented at the Annual Meetings of the Association for Research in Vision and Ophthalmology and the Society for Information Display. A more extensive treatment may be found in the first author's Ph.D. dissertation.[88]

Address correspondence to Paul Beckmann at the address on the title page or by e-mail at paul @eye.psych.umn.edu.

REFERENCES AND NOTES

1. P. Artal, I. Iglesias, N. López-Gil, and D. G. Green, "Double-pass measurements of the retinal-image quality with unequal entrance and exit pupil sizes and the reversibility of the eye's optical system," J. Opt. Soc. Am. A **12**, 2358–2366 (1995).
2. F. W. Campbell and R. W. Gubisch, "Optical quality of the human eye," J. Physiol. (London) **186**, 558–578 (1966).
3. A. Guirao and P. Artal, "Off-axis monochromatic aberrations estimated from double pass measurements in the human eye," Vision Res. **39**, 207–217 (1999).
4. R. Navarro, P. Artal, and D. R. Williams, "Modulation transfer function of the human eye as a function of retinal eccentricity," J. Opt. Soc. Am. A **10**, 201–212 (1993).
5. L. N. Thibos, A. Bradley, D. L. Still, X. Zhang, and P. A. Howarth, "Theory and measurement of ocular chromatic aberration," Vision Res. **30**, 33–49 (1990).
6. C. A. Curcio, K. R. Sloan, R. E. Kalina, and A. E. Hendrickson, "Human photoreceptor topography," J. Comp. Neurol. **292**, 497–523 (1990).
7. C. A. Curcio, K. R. Sloan, and D. Meyers, "Computer methods for sampling, reconstruction, display and analysis of retinal whole mounts," Vision Res. **29**, 529–540 (1989).
8. B. Chen, W. Makous, and D. R. Williams, "Serial spatial filters in vision," Vision Res. **33**, 413–427 (1993).
9. C. A. Curcio, K. A. Allen, K. R. Sloan, C. L. Lerea, J. B. Hurley, I. B. Klock, and A. H. Milam, "Distribution and morphology of human cone photoreceptors stained with anti-blue opsin," J. Comp. Neurol. **312**, 610–624 (1991).
10. D. H. Brainard, A. Roorda, Y. Yamauchi, J. B. Calderone, A. Metha, M. Neitz, J. Neitz, D. R. Williams, and G. H. Jacobs, "Function consequences of the relative numbers of L and M cones," J. Opt. Soc. Am. A **17**, 607–614 (2000).
11. H. Wässle, "Retinal ganglion cell density and cortical magnification factor in the primate," Vision Res. **30**, 1897–1911 (1990).
12. S. T. L. Chung, J. S. Mansfield, and G. E. Legge, "Psychophysics of reading XVIII. The effect of print size on reading speed in normal peripheral vision," Vision Res. **38**, 2949–2962 (1998).
13. G. E. Legge, J. S. Mansfield, and S. T. L. Chung, "Psychophysics of reading XX. Linking letter recognition to reading speed in central and peripheral vision," Vision Res. **41**, 725–743 (2001).
14. S. M. Anstis, "A chart demonstrating variations in acuity with retinal position," Vision Res. **14**, 589–592 (1974).
15. E. Ludvigh, "Extrafoveal visual acuity as measured with Snellen test-letters," Am. J. Ophthalmol. **24**, 303–310 (1941).
16. A. M. Jacobs, T. A. Nazir, and O. Heller, "Perception of lowercase letters in peripheral vision: a discrimination matrix based on saccade latencies," Percept. Psychophys. **46**, 95–102 (1989).
17. M. Millodot, C. A. Johnson, A. Lamont, and H. W. Leibowitz, "Effect of dioptrics on peripheral visual acuity," Vision Res. **15**, 1357–1362 (1975).
18. J. M. White and D. S. Loshin, "Grating acuity overestimates Snellen acuity in patients with age-related maculopathy," Optom. Vision Sci. **66**, 751–755 (1989).
19. H. Bouma, "Visual recognition of isolated lower-case letters," Vision Res. **11**, 459–474 (1971).
20. B. E. Roethlein, "The relative legibility of different faces of printing types," Am. J. Psychol. **23**, 1–36 (1912).
21. E. C. Sanford, "The relative legibility of the small letters," Am. J. Psychol. **1**, 402–435 (1888).
22. K. R. Alexander, W. Xie, and D. J. Derlacki, "Visual acuity and contrast sensitivity for individual Sloan letters," Vision Res. **37**, 813–819 (1997).
23. R. S. Anderson and L. N. Thibos, "Relationship between acuity for gratings and for tumbling-E letters in peripheral vision," J. Opt. Soc. Am. A **16**, 2321–2333 (1999).
24. W. S. Geisler, "Sequential ideal-observer analysis of visual discriminations," Psychol. Rev. **96**, 267–314 (1989).
25. W. S. Geisler, "Physical limits of acuity and hyperacuity," J. Opt. Soc. Am. A **1**, 775–782 (1984).
26. W. S. Geisler and K. D. Davila, "Ideal discriminators in spatial vision: two-point stimuli," J. Opt. Soc. Am. A **2**, 1483–1497 (1985).
27. W. S. Geisler and D. B. Hamilton, "Sampling-theory analysis of spatial vision," J. Opt. Soc. Am. A **3**, 62–70 (1986).
28. M. S. Banks, A. B. Sekuler, and S. J. Anderson, "Peripheral spatial vision: limits imposed by optics, photoreceptors, and receptor pooling," J. Opt. Soc. Am. A **8**, 1775–1787 (1991).
29. G. E. Legge, S. J. Ahn, T. S. Klitz, and A. Luebker, "Psychophysics of reading XVI. The visual span in normal and low vision," Vision Res. **37**, 1999–2010 (1997).
30. H. E. Blanchard, A. Pollatsek, and K. Rayner, "The acquisition of parafoveal word information in reading," Percept. Psychophys. **46**, 85–94 (1989).
31. G. E. Legge, G. S. Rubin, D. G. Pelli, and M. M. Schleske, "Psychophysics of reading II. Low vision," Vision Res. **25**, 253–266 (1985).
32. K. Rayner and J. H. Bertera, "Reading without a fovea," Science **206**, 468–469 (1979).
33. The photoreceptors were positioned on a regular, triangular close-packed grid. Photons were captured by the photoreceptor if they fell anywhere in their physiologic aperture, which was taken to be a circle with a diameter equal to the cone spacing. The retinal image was sampled by this mosaic by multiplying it by the Fourier transform of a single cone, inverse transforming the result, and sampling the image at the known receptor sites.
34. Geisler derived a closed-form expression for the likelihood computed from the mean absorption counts for both of the alternatives.

35. Their study controlled the optical image quality of the eye across the visual field by using an external 1.5-mm pupil. They used such a pupil in the human experiments and represented the imaging in the model as diffraction limited.
36. G. Westheimer, "The eye as an optical instrument," in *Handbook of Perception and Human Performance. Vol. I. Sensory Processes and Perception*, K. R. Boff, L. Kaufman, and J. P. Thomas, eds. (Wiley, New York, 1986), pp. 4-1–4-20.
37. The photoreceptors were positioned on a regular triangular mosaic at the densities found by Curcio and her colleagues,[6] and the aperture of the photoreceptor was taken as either the diameter of the inner segment or the outer segment of the receptor, with a photon taken as captured if it fell anywhere within the aperture. The isomerization rate was taken as eccentricity dependent.
38. The location of each cone is known exactly by the decision stage.
39. D. G. Pelli, "The quantum efficiency of vision," in *Vision: Coding and Efficiency*, C. Blakemore, ed. (Cambridge U. Press, 1990), pp. 3–24.
40. J. A. Solomon and D. G. Pelli, "The visual filter mediating letter identification," Nature **369**, 395–397 (1994).
41. Two parameters that affect the rendering of the letter on the display will be considered here: *pixel pitch* defined as the physical separation between adjacent pixels, and *pixel width* defined as the standard deviation of the Gaussian pixel profile. The pixels are arranged on a rectangular grid.
42. W. Cowan, "Displays for vision research," in *Handbook of Optics. Vol. I: Fundamentals, Techniques, and Design*, M. Bass, ed. (McGraw-Hill, New York, 1995), pp. 27.1–27.44.
43. J. Santamaría, P. Artal, and J. Bescos, "Determination of the point-spread function of human eyes using a hybrid optical-digital method," J. Opt. Soc. Am. A **4**, 1109–1114 (1987).
44. The PSF includes the effects of defocus, chromatic aberration, diffraction, and scatter. For our study the reported modulation transfer function values of Navarro *et al.*[4] were used to estimate the PSF. The horizontal and vertical cross sections of the PSF were each modeled as the sum of two Gaussians. Fitting the PSF with Gaussians provided a straightforward computation of the retinal image of a 2D Gaussian pixel. The area under the PSF was normalized to 1.0 while the relative contributions of these two Gaussians and their standard deviations were varied with eccentricity. In the simulations reported here, astigmatism was not included for the following reasons. Central astigmatism varies within the human population and between the eyes of individuals.[45] In addition, the effects of peripheral astigmatism are quite small within 20° of central vision.[46] The relationship between central and peripheral astigmatism initially appeared to vary in complex ways that differ significantly between individuals.[4] Artal and his colleagues, however, recently developed a technique that allows investigation of odd-order aberrations, including peripheral astigmatism.[1,3] They found that peripheral astigmatism and coma were most consistent between subjects but that peripheral defocus varied greatly between subjects. The position of Williams[47] and Guirao and Artal[3] is that the circle of least confusion remains unchanged at least out to 20°. This compromise condition of focus is the one included here.
45. A. M. McKendrick and N. A. Brennan, "Distribution of astigmatism in the adult population," J. Opt. Soc. Am. A **13**, 206–214 (1996).
46. W. Lotmar and T. Lotmar, "Peripheral astigmatism in the human eye: experimental data and theoretical model predictions," J. Opt. Soc. Am. **64**, 510–513 (1974).
47. D. R. Williams, P. Artal, R. Navarro, M. J. McMahon, and D. H. Brainard, "Off-axis optical quality and retinal sampling in the human eye," Vision Res. **36**, 1103–1114 (1996).
48. The model uses the field scale values of 282, 277, and 262 μm/deg at 0°, 5°, and 20° eccentricity to determine the size of the stimulus image on the retina. These field scales have been calculated by using the Drasdo[49] wide-field schematic eye following Curcio.[50]
49. N. Drasdo and C. W. Fowler, "Non-linear projection of the retinal image in a wide-angle schematic eye," Br. J. Ophthamol. **58**, 709–714 (1974).
50. C. A. Curcio and K. R. Sloan, "Packing geometry of human cone photoreceptors: variation with eccentricity and evidence for local anisotropy," Visual Neurosci. **9**, 169–180 (1992).
51. W. N. Charman, "Optics of the human eye," in *Vision and Visual Dysfunction, Vol. 1, Visual Optics and Instrumentation*, W. N. Charman, ed. (Macmillan, London, 1991), pp. 1–26.
52. L. N. Thibos, "Calculation of the influence of lateral chromatic aberration on image quality across the visual field," J. Opt. Soc. Am. A **4**, 1673–1680 (1987).
53. P. A. Howarth and A. Bradley, "The longitudinal chromatic aberration of the human eye, and its correction," Vision Res. **26**, 361–366 (1986).
54. C. A. Curcio, University of Alabama at Birmingham; 700 South 18th Street, Room H20; Birmingham, Alabama 35294-0009 (personal communication, October 6, 1993).
55. S. Marcos, R. Navarro, and P. Artal, "Coherent imaging of the cone mosaic in the living human eye," J. Opt. Soc. Am. A **13**, 897–905 (1996).
56. C. M. Cicerone and J. L. Nerger, "The relative numbers of long-wavelength-sensitive to middle-wavelength-sensitive cones in the human fovea centralis," Vision Res. **29**, 115–128 (1989).
57. P. D. Gowdy, S. Otake, and C. M. Cicerone, "The spatial arrangement of L and M cones in the living human eye," Vision Res. Suppl. **37**, S448 (1996).
58. J. L. Nerger and C. M. Cicerone, "The ratio of L cones to M cones in the human parafoveal retina," Vision Res. **32**, 879–888 (1992).
59. C. M. Cicerone and S. Otake, "Color-opponent sites: individual variability and changes with retinal eccentricity," Invest. Ophthalmol. Visual Sci. Suppl. **38**, S454 (1997).
60. A. Roorda and D. R. Williams, "The arrangement of the three cone classes in the living human eye," Nature **397**, 520–522 (1999).
61. S. Otake, P. D. Gowdy, and C. M. Cicerone, "The spatial arrangement of L and M cones in the peripheral human retina," Vision Res. **40**, 677–693 (2000).
62. Each cone class is assumed to have a fixed probability of absorption for all quanta entering its aperture, based on the wavelength of the light and the cone class. Some evidence of individual differences in the photopigment density, at least near the fovea,[63] exists. This difference, however, is not incorporated into the model. Instead, a peak absorption probability of 50% is assumed in the calculations.
63. M. W. Levine, R. P. Zimmerman, and V. Carrion-Carire, "Variability in responses of retinal ganglion cells," J. Opt. Soc. Am. A **5**, 593–597 (1988).
64. G. Wyszecki and W. S. Stiles, *Color Science*, 2nd ed. (Wiley, New York, 1982).
65. Psychophysical studies of cone vision[66] have shown that quantum noise follows Poisson statistics in the dark-adapted human eye.
66. K. Donner, "Noise and the absolute thresholds of cone and rod vision," Vision Res. **32**, 853–866 (1992).
67. J. T. Tou and R. C. Gonzalez, *Pattern Recognition Principles* (Addison-Wesley, Reading, Mass., 1974).
68. M. S. Banks, W. S. Geisler, and P. J. Bennett, "The physical limits of grating visibility," Vision Res. **27**, 1915–1924 (1987).
69. The Gabor patch was rendered as a 101×101 pixel bitmap representing a cosinusoidal horizontal grating modulated by a 2D circular half-cosine envelope. The half-cosine spanned 7.5 periods of the underlying grating. Each period of the grating was rendered across 12.5 pixels. The spatial frequency of the grating was changed by changing the viewing distance and keeping the rendering of the grating the same. The amplitude of the grating modulation of the background was changed for each distance until the model performed at threshold level.

70. The cutoff due to diffraction is 110 cpd for a 4-mm pupil. It is reasonable to expect the 4-mm pupil diameter represented in the current model to exhibit a cutoff higher than that of the 1.5-mm pupil used by Banks but lower than the theoretical diffraction limit due to aberrations.
71. L. L. Sloan, "The photopic acuity-luminance function with special reference to parafoveal vision," Vision Res. **8**, 901–911 (1968).
72. F. L. van Nes and J. C. Jacobs, "The effect of contrast on letter and word recognition," IPO Ann. Prog. Rep. **16**, 72–80 (1981).
73. K. R. Alexander, D. J. Derlacki, G. A. Fishman, and J. P. Szlyk, "Temporal properties of letter identification in retinitis pigmentosa," J. Opt. Soc. Am. A **10**, 1631–1636 (1993).
74. W. Seiple, K. Holopigian, Y. Shnayder, and J. P. Szlyk, "Duration thresholds for target detection and identification in the peripheral visual field," Optom. Vision Sci. **78**, 169–176 (2001).
75. Postscript™ assigns an origin within its definition for each letter. Within each x-height size, the origin of the letters was in the same location, trial to trial. Alternative rules for aligning stimulus letters on the screen could influence performance of the ideal observer; for instance, in an extreme case in which the 26 letters were presented at distinct, nonoverlapping regions of the screen, the ideal-observer's performance would be significantly improved. The method used here, however, resulted in substantial overlap between the letter images.
76. K. R. Aggarwala, S. Nowbotsing, and P. B. Kruger, "Accommodation to monochromatic and white-light targets," Invest. Ophthalmol. Visual Sci. **36**, 2695–2705 (1995).
77. P. B. Kruger and J. Pola, "Stimuli for accommodation: blur, chromatic aberration and size," Vision Res. **26**, 957–971 (1986).
78. D. H. Foster and W. F. Bischof, "Thresholds from psychometric functions: Superiority of bootstrap to incremental and probit variance estimators," Psychol. Bull. **109**, 152–159 (1991).
79. L. T. Maloney, "Confidence intervals for the parameters of psychometric functions," Percept. Psychophys. **47**, 127–134 (1990).
80. W. H. Press, B. P. Lannery, S. A. Teukolsky, and W. T. Vetterling, *Numerical Recipes in C: The Art of Scientific Computing* (Cambridge U. Press, New York, 1988).
81. This presentation time was chosen because it was the shortest reliable presentation time possible with the software and hardware used in the experiment.
82. R. M. Steinman, G. M. Haddad, A. A. Skavenski, and D. Wyman, "Miniature eye movements," Science **181**, 810–819 (1973).
83. B. S. Tjan, "Ideal observer analysis of object recognition," Ph.D. dissertation (University of Minnesota, Minneapolis, Minn., 1996).
84. B. S. Tjan, W. L. Braje, G. E. Legge, and D. Kersten, "Human efficiency for recognizing 3-D objects in luminance noise," Vision Res. **35**, 3053–3069 (1995).
85. Tjan measured percent-correct identification performance as a function of SNR for letters of fixed size. Our work uses letters of fixed contrast and letters of varying size. It is possible, however, to build a bridge between these two approaches by noting that "signal" for the ideal observer used by Tjan is proportional to the square of letter x height for fixed contrast. Thus a factor of k increase in SNR at threshold performance in Tjan's analysis corresponds to a $k^{0.5}$ increase in letter size at fixed contrast and the same threshold level of performance. We used this method to calculate our estimates.
86. G. E. Legge and J. M. Foley, "Contrast masking in human vision," J. Opt. Soc. Am. **70**, 1458–1471 (1980).
87. C. A. Curcio and K. A. Allen, "Topography of ganglion cells in human retina," J. Comp. Neurol. **300**, 5–25 (1990).
88. P. J. Beckmann, "Preneural limitations to identification performance in central and peripheral vision," Ph.D. dissertation (University of Minnesota, Minneapolis, Minn., 1998).